Extrusion foaming of linear and branched polypropylenes – input of the thermomechanical analysis of pressure drop in the die

Carlos Sandino, Edith Peuvrel-Disdier, Jean-François Agassant, Patrice Laure, Séverine A.E. Boyer, Geoffrey Hibert, Yves Trolez

Extrusion foaming of linear and branched polypropylenes

- Input of the thermomechanical analysis of pressure drop in the die

C. Sandino[1], E. Peuvrel-Disdier[1*], J.F. Agassant[1], P. Laure[1,2], S.A.E. Boyer[1],

G. Hibert[3], Y. Trolez[3]

[1] MINES Paris - PSL, CEMEF – Centre de Mise en Forme des Matériaux, UMR CNRS 7635, CS 10207, 06904 Sophia Antipolis (France)

[2] Laboratoire J.-A. Dieudonné, CNRS UMR 6621, Université Côte d'Azur, Parc Valrose, 06108 Nice Cedex 02 (France)

[3] TotalEnergies One Tech Belgium, Zone Industrielle Feluy C, B 7181 Feluy (Belgium)

* Corresponding author: edith.peuvrel-disdier@minesparis.psl.eu

Abstract:

This paper aims at a better understanding of the polypropylene (PP) physical extrusion foaming process with the objective of obtaining the lowest possible foam density. Two branched PP have been compared to the corresponding linear ones. Their shear and elongation viscosities have been measured as well as their crystalline properties.

Trials were conducted in a single screw extruder equipped with a gear pump and a static mixer cooler to adjust the melt temperature at the final die. The effect of decreasing this temperature on the PP foamability and on the pressure drop in the die was analyzed.

The foam density of branched PPs varies from high to low values while decreasing the foaming temperature. In the same processing conditions, the foam density of linear PPs does not decrease so much as already evidenced in the literature. The foamability transition coincides with an increase of the pressure drop in the die.

The originality of the work lies in the thermomechanical analysis of the polymer flow in the die which allows the identification of the relevant physical phenomena for a good foamability. The comparison of the experimental pressure drops in the die and the computed ones with the identified purely viscous behavior points out the influence of the foaming temperature and of the polypropylene structure. At high foaming temperature the discrepancy between experimental measurements and the computed pressure drops remains limited. It increases when decreasing the foaming temperature, but the mismatch is much more important for branched PPs than for linear ones. This difference is analyzed as a combination of the activation energy of the viscosity, the elongational viscosity in the convergent geometry of the die which is much more important for branched PPs than for linear ones and the onset of crystallization which occurs at higher temperature for branched PPs than for linear PPs.

Keywords: Extrusion foaming, polypropylene, thermomechanical analysis, chain architecture

1) Introduction

Polymer and in particular thermoplastic foams are of great industrial interest since low foam densities can be obtained without major compromise on mechanical properties. Low polymer foam densities refer to densities lower than 0.2 and high foam densities to densities larger than 0.5. Because of outstanding characteristics (higher strength than polyethylene, better impact strength than polystyrene, high service temperature, excellent chemical resistance, recyclability) and low material cost, PP foams can be foreseen as a good substitute to other polymer foams. Microcellular foams with a cell density larger than 10^9 cells/cm^3 or a cell size in the order of 10 microns can be effective materials for thermal insulation, cushioning, packaging (wedging particles for transportation), structural materials for aerospace/automotive and many sporting applications. The foam density is a first order parameter to determine a polymer ability to foaming. However structural parameters, such as the cell density, the mean bubble size, the bubble size distribution, the volume fraction of closed and open cells, are also important to better characterize the polymer foamability but also its ability regarding a given application. For example, closed cell foams with the right cell size are better adapted for thermal insulation, whereas open cell foams with interconnected cells are better suited for acoustic absorption applications. But standard PPs suffer from a low melt strength and a narrow foaming temperature window of a few degrees. For this reason, many studies were and are still conducted on one side to improve the PP melt strength and extensibility by tuning the chain architecture (i.e. use of long chain branching PP, blending of PPs with different molecular structures, cross-linking…) but also tuning the foaming process (die geometry, process conditions) to increase the foamability window and reduce the cell coalescence. Examples of studies are given in the following.

Batch discontinuous foaming process has been used to study the nucleation and bubble growth mechanisms and define the foamability windows for various polymers. Guo *et al.* (2006) used a high-pressure vessel which can impose pressure drop ratios as high as $2.5\ \mathrm{GPa}/s$. Transparent windows allow observing the nucleation and bubble growth mechanisms in polystyrene (PS) with carbon

dioxide (CO_2) as a blowing agent. It is shown that a higher pressure drop rate induces finer cells and a higher cell density. Xu *et al.* (2007) studied the foaming ability of a linear polypropylene (PP) with supercritical carbon dioxide (SC CO_2) in the same kind of batch system. The effects of saturation time, foaming temperature, saturation pressure and depressurization rate on the foam structure and volume expansion ratio were investigated. A very narrow temperature range and an optimal depressurization rate were identified. With the same (PP/ SC CO_2) mixture, Li *et al.* (2011) reported the plasticization effect of (SC CO_2) as well as a sharp decrease of the crystallization temperature which allows to produce low density foams in a wide temperature range. Raps *et al.* (2014) also showed a crystallization temperature decrease with the gas loading as well as a sharp decrease of the PP viscosity. In a review paper, Mohebbi *et al.* (2015) investigated the respective influence of nucleating agents and long chain branching on polypropylene foamability. Zhang *et al.* (2019) used a mixture of CO_2 and isobutane for Low Density Polypropylene (LDPE) foaming. Guo *et al.* (2020) used their transparent batch foaming system to compare the linear and branched PP foaming processes with CO_2 blowing agent. Rainglet *et al.* (2021) studied the foaming ability with CO_2 of a maleic anhydride-grafted PP which develops long branches by reactive extrusion.

Several extrusion disposals have been used for foaming with chemical and physical blowing agents. Park *et al.* (1995) used a single screw extruder connected with dies of different geometries to produce high impact PS foams with CO_2 or nitrogen as blowing agent. They showed how the die geometry influences the bubble size distribution in the extrudate. Naguib *et al.* (2002) used a tandem of single screw extruders (the first one to achieve PP melting and the second one to introduce butane as foaming agent) followed by a static mixer to reduce the melt temperature. They pointed out the existence of an optimal temperature of the static mixer which decreases with an increase of gas content. The achieved foam density with branched PPs was significantly lower than with linear PPs. Using the same process, Naguib *et al.* (2004) showed how gas loss and PP crystallization govern the foaming rate. Spitael and Macosko (2004) used a twin-screw extruder which allows introducing CO_2

directly after the melting screw elements. They used different linear and branched PPs as well as blends of linear and branched chains. Refined foam structures were obtained with high pressure drop rates. The difference between linear and branched PP was not as marked as in the previous studies. Xu *et al.* (2005) used CBA to directly produce CO_2 in a single screw extruder. They were able to produce low density foams, even with linear PP, but using crosslinking agents. In a book chapter, Ramesh (2014) reviewed the different extrusion foaming processes of polyolefins. Salmang and Pinsolle (2014) published a technical review on the extrusion foaming process of PS. They showed that the foamed extrudate can collapse at a too high extrusion temperature. Lee and Park (2014) published a second edition on polymer extrusion foaming in which all the bibliography is collected.

The parameters, pressure, temperature and initial gas concentration, determine the soluble gas concentration available for the foaming. The die geometry affects the pressure drop rate in the die and thus the cell density. The processing window is a balance between the foaming temperature defining the melt strength and the time to crystallization. Di Maio and co-workers (Ianniello *et al.,* 2022) recently proposed a heuristic approach to determine the polymer foamability during the last stages of the foaming process (bubble impingement and foam setting). Three possible physical mechanisms are identified as favorable for a good foamability: a large viscosity increase for a temperature reduction, strain hardening and flow-induced crystallization. They proposed to use the strain during the foaming process as an indicator to determine if one or several of these mechanisms can be active or not. However, a realistic scenario of the extrusion physical foaming process, considering the pressure drop and temperature along the process, as well as the materials physics, such as strain hardening and crystallization, still needs advanced works.

In this paper we investigated the physical extrusion foaming of several PPs, linear and branched, with CO_2, with the objective of obtaining the lowest foam density. The shear and elongation rheology as well as the crystallization temperatures of the different PPs have been characterized. Foaming experiments were conducted at a fixed gas content and the same extrusion conditions. The foaming

temperature was systematically decreased before the die thanks to a static mixer/cooler. The objective was to correlate the effect of decreasing the foaming temperature on PP foamability and the recorded pressure profile in the case of linear and branched chains. The polymer foamability was characterized via the measurement of foam densities and structural observations by scanning electronic microscopy (SEM). A detailed thermomechanical analysis of the polymer flow in the extrusion die was conducted using the identified rheology. The comparison of the experimental and computed pressure drop variation with the foaming temperature for the different PPs allows to propose a realistic scenario for the foaming process, combining the temperature dependence of the viscosity, strain hardening and crystallization development. This allows discriminating the extrusion foamability of the investigated linear and branched PPs.

2) Characterisation of the Linear and Branched Polypropylenes

Four experimental grades of PP, synthesized by TotalEnergies, were used in this study. Two grades are based on homopolymer chains, referred as PPH, and the other two are based on random copolymers, referred as PPR. PPH and PPR grades are composed of a linear grade (respectively PPH-L, PPR-L grades) and its respective long chain branching grade (respectively PPH-B, PPR-B grades). All the PPs are based on a metallocene synthesis process according (Welle et al., 2022). Grades were selected so that the linear grades on one side and the branched grades on the other side, respectively, almost have the same rheological behavior (see Figures 1 and 2).

The dynamic rheology of the different PPs has been measured on an ARES-RDA strain-controlled rheometer from T.A. Instruments (USA) using a $25\,mm$ diameter plate-and-plate geometry ($1.6 - 2\,mm$ gap). Measurements were performed at three temperatures in the temperature range (150-185°C). According to Cox-Merz principle (Cox and Merz, 1958), the shear viscosity is equivalent to the dynamic one. Figure 1 compares the shear viscosity curves of the different PPs at a common temperature of 170°C.

Figure 1

The viscosity of both PPH is slightly higher than the viscosity of both PPR. The rheological behavior of linear and branched polymers is quite different with a more pronounced shear-thinning behaviour for branched PPs over the reported frequency range and a Newtonian plateau shifted to lower frequencies and higher viscosities, and a smooth transition between the Newtonian plateau and the shear-thinning behaviour for the linear PPs. The rheology curves have been fitted with a Carreau-Yasuda constitutive equation (Carreau, 1972; Yasuda *et al.*, 1981) or a power law which will be used latter in the thermomechanical analysis:

$$\eta = \eta_0 \left[1 + (\lambda \dot{\gamma})^b\right]^{\frac{m-1}{b}} \quad (1)$$

$$\eta = K_0 \dot{\gamma}^{m-1} \quad (2)$$

where η_0 is the Newtonian (or zero shear-rate) viscosity, λ the relaxation time, $\dot{\gamma}$ the shear rate, a the Yasuda coefficient controlling the transition between Newtonian plateau and power law region, m the shear thinning or power law index, K_0 the consistency. Note that λ is the inverse of the shear rate at which the fluid changes from Newtonian to shear-thinning behavior. The temperature dependence of the rheological data is integrated via a shift factor a_T following an Arrhenius law:

$$a_T = \exp\left[\frac{E_a}{\mathcal{R}}\left(\frac{1}{T} - \frac{1}{T_{\text{ref}}}\right)\right] \quad (3)$$

where $\mathcal{R}$ is the ideal gas constant, E_a is the polymer activation energy, T_{ref} is the reference temperature. The identified coefficients are reported in Table 1. The power law parameters are identified from viscosity data corresponding to a shear-rate greater than $10\ s^{-1}$.

Table 1

The activation energy E_a of the branched polymers is slightly higher than the one of linear polymers which implies a sharper viscosity increase when decreasing the foaming temperature. The gas diffusion coefficient decreases (limiting gas escape for a more efficient foaming) with the temperature decrease, which means when the viscosity increases. This relaxation time λ is ten times higher for the branched PPs and this is the signature of their marked viscoelastic character (Vega *et al.*, 2009).

The elongational viscosity has been measured on an ARES-EVF from T.A. Instruments (USA) at a constant elongation rate ($0.1\ s^{-1}$) in a temperature range which is adjusted for each polypropylene. Experimental data are then plotted in Figure 2 at the same temperature (170°C) using the same time temperature superposition as for the shear rheology. The elongational behavior of the linear and branched polymers are of course different. A sharp strain hardening is observed for both branched polymers. The linear grades do not present any strain hardening. Their transient behaviour presents an overshoot before reaching the steady viscosity plateau. The occurrence of an overshoot/maximum or not during the transient extensional behavior was debated in the literature and appears to be most likely due to artefacts (e.g. nonuniformity of the sample deformation during the test) (Münstedt and Stary, 2013). Steady state elongational viscosities (although with some uncertainties) remain in the right order of magnitude when comparing with the Troutonian viscosities (calculated from shear viscosities).

Figure 2

The dissolved gas in the polymer plays the role of a plasticizer. Therefore, a shift factor a_G can also be considered (Raps *et al.*, 2014). The a_G factor can be determined from capillary measurements performed on slit dies in the presence of gas (Raps *et al.,* 2017). In this way, an empirical law is exhibited and gives the variation of the shift factor with the gas weight fraction wt_g :

$$\log_{10} a_g = A\, wt_g + B \qquad (4)$$

From Figure 7 in (Raps *et al.,* 2014), one gets $A = -0.074$ and $B = -0.038$ if the gas concentration is expressed in term of weight fraction (wt%).

Shift factors of temperature $a_T(T)$ and gas concentration a_g (influence of pressure neglected) can be combined to a general shift factor $a = a_T(T)\, a_g(wt_g)$. The integration of the shift factors in the Carreau-Yasuda or power law results in Eqs. 5 and 6:

$$\eta(T,\dot{\gamma}) = a\, \eta_0\, [1 + (a\, \lambda\, \dot{\gamma})^b]^{\frac{m-1}{b}} \qquad (5)$$

$$\eta\,(T,\dot{\gamma}) = a^m\ K_0\,\dot{\gamma}^{m-1} \quad (6)$$

The crystalline properties of the different polypropylenes have been analysed using DSC experiments. Calorimetry measurements were performed on a Mettler Toledo DSC 1 STAR^e System at $10℃/mn$ with a first melting up to 200°C to erase all traces of crystals, followed by a cooling at the same rate. The homopolymer and copolymer grades mainly differ by their crystalline properties with marked differences in crystallization temperatures and enthalpies (Table 2). DSC curves are presented in Annex. Homopolymers PPH grades crystallize at higher temperatures and present a higher crystalline fraction (higher enthalpy of crystallization) than random copolymer PPR grades. Branched polymers crystallize at a higher temperature than linear ones (around 10°C difference for PPH and only a few degrees difference for PPR) (Vega *et al.*, 2009).

Table 2

3) Foaming Process

3.1 Experimental set up

A single-screw extruder (Barmag 6E4, screw diameter $60\,mm, L/D = 40$) equipped with a gear pump was used to melt the PP and incorporate the gas. The CO_2 is injected in the metering zone of the single screw extruder at $S_0 = 1.05$ wt%. The gear pump allows setting a constant flow rate. A static mixer coupled with an efficient cooling system allows adjusting the final melt temperature between 165°C and 130°C before foaming. This temperature T_{m} is referred as the foaming temperature in the following. The polymer is finally forced through a capillary die. Pressures and temperatures are recorded along the single-screw barrel, after the gear pump, in the melt cooler static mixer and at die entrance (Figure 3).

Figure 3

The rod die geometry consists of a conical convergent followed by a very short capillary die to ensure a high and localized pressure drop just before die exit (Figure 4). Dimensions are reported in Table 3. The overall strain may be approximated by (Padmanabhan and Macosko, 1997):

$$\varepsilon_{\max} = \ln(R_1^2/R_0^2) \quad (6)$$

This Hencky strain is therefore equal to 5.6 in the present study which corresponds to a marked stain hardening phenomenon in the case of branched polymers (Figure 2).

Figure 4

Table 3

3.2 Processing conditions

The same flow rate (2.9 kg/h) as well as the same gas content (1.05 wt%) was used in all experiments. The single screw barrel temperature and the gear pump temperature were set constant (Table 4). The temperature was progressively decreased in the static mixer cooler (between thermocouples T_7 and T_8) to reach the foaming temperature at the die exit (T_{m}).

Table 4

Figure 5 shows the pressure profile along the extruder for different foaming temperatures with the branched PPR. The pressure profiles are quite similar for all trials up to the pressure sensor P_5 .This sensor is located between the gas injection port and the gear pump (Figure 3). The pressure profiles are considerably different after the gear pump (P_6 sensor) at the static mixer entrance (P_7 sensor) and obviously at the die entrance (P_8 sensor), depending on the foaming temperature. Pressure P_6 increases regularly when decreasing the set temperature of the static mixer melt cooler. Similar pressure profiles are observed for the branched PPH as well as for both linear PPs.

Figure 5

3.3: Influence of the processing conditions on the foam density

Foams densities were systematically measured on the extrudates and used to define the polymer foamability. This density was measured on a hydrostatic balance following Archimedes principle.

The theoretical lowest density ρ_{th} can be calculated from the injected amount of gas in the polymer and the remained dissolved gas at the die exit. The gas was injected just before the gear pump, at a pressure of 16 MPa and a temperature around 200 °C (Figure 5). The maximum weight fraction of gas S which can be dissolved in the molten polymer is described by Henry's law:

$$S = H_p P \tag{7}$$

where H_p is the Henry constant and P the pressure. If the solubility, S is defined as percentage of weight fraction (mass gas/mass polymer), the unity of Henry constant H_p is (wt%/Pa) and can be described with the Van't Hoff equation at different temperatures:

$$\ln(H_p) = \ln(H_0) + \left(\frac{-\Delta H_{\mathrm{sol}}}{R\,T}\right) \tag{8}$$

From data of Areerat *et al.* (2004) (Table 5), one obtains $S(200°\mathrm{C},\ 16\ \mathrm{MPa}) = 10$ wt% which means that the total amount of $S_0 = 1.05$ wt% is dissolved in the polymer. At the die exit, the pressure is around 0.1 MPa and the temperature between 130°C and 150°C and therefore S is between 0.08 and 0.09 wt%. Finally, the lowest density ρ_{th} which can be obtained with an initial amount S_0 of CO_2 dissolved in the polymer is given by:

$$\rho_{\mathrm{th}} = \frac{\rho_{\mathrm{PP}}\left(1+\frac{S_0}{100}\right)}{\left(1+\frac{(S_0 - H_p(T_{\mathrm{m}})\,P_{\mathrm{amb}})}{100}\frac{\rho_{\mathrm{PP}}}{M_{\mathrm{CO_2}}}\frac{R\,T_{\mathrm{m}}}{P_{\mathrm{atm}}} + \frac{\rho_{\mathrm{PP}}}{\rho_{\mathrm{CO_2}}}\frac{H_p(T_{\mathrm{m}})\,P_{\mathrm{atm}}}{100}\right)} \tag{9}$$

where P_{atm} is the atmospheric pressure. This lowest density is in the range $117 - 126$ kg/m^3.

Table 5

Therefore, the objective was to produce low foam densities close to the target value ρ_{th} calculated from the amount of gas S_0 added to the polymer represented by a dashed line in Figure 6. Other foam characteristics as mean cell size, cell size distribution, open/closed cells have not been investigated. As observed in Figure 5 (insert), the pressure profiles corresponding to bad foamability

(dashed red lines) are related to high foaming temperatures (T_m). These pressure profiles remain below the good foamability profiles (blue solid lines). High foaming temperatures corresponding to low pressures ($1.3 \leq \Delta P_8 \leq 1.6$ MPa) are related to bad foamability and low foaming temperatures with high pressures ($2.0 \leq \Delta P_8 \leq 4.5$ MPa) related to good foamability. To clarify the relation between polymer foamability and pressure drop in the die and foaming temperature, the foam density of the four PP grades is represented versus the pressure drop between die entrance and die exit ΔP_8 (Figure 6).

Figure 6

Decreasing the foaming temperature induces an increasing pressure drop which, in turn, results in a lower foam density. This is clearly visible in Figure 6.b for PPR-B. When decreasing the temperature from 144 to 136 °C, the pressure at die entrance increases from 2 to 4.5 MPa and the foam density increases slightly from 152 to 182 kg/m^3. When the temperature is larger than 144°C, the pressure decreases, and the foam density increases markedly (600 kg/m^3 at 161°C). SEM pictures of PPR-B foams in different foaming conditions are presented in Figure 7. It is to notice that, even if the density is quite equivalent for foaming temperatures at 138°C or 144°C, the foam morphologies are quite different with a finer structure at the lowest temperature.

Figure 7

The same phenomenon is observed in Figure 6 for PPH-B and a good foamability may be obtained for even lower pressure drops (1.7 MPa) and higher temperature ($T_m < 155$°C). At T=154°C (Figure 8a) one observes a low foam density for PPH-B (151 kg/m^3). It was not possible to achieve such a low density with PPR-B at the same temperature.

Figure 8

This good foamability could not be achieved for the linear products (Figure 8b). The foaming temperature ranges obtained for these grades are not low enough for producing a pressure drop that

ensures good foamability. Nevertheless, for PPR-L (Figure 6a), it was possible to decrease the temperature to $T_m = 130°C$ which results in an important increase of the pressure drop and, therefore an important decrease of the foam density, but not low enough to be considered as a good foam. Extrusion trials with lower foaming temperatures could not be conducted because of the crystallization of the polymer in the final die which blocks the screw rotation.

These results confirm that the processing window to obtain a low-density polypropylene foam is narrow, even with an adjusted macromolecular architecture.

4) Thermomechanical analysis of the foaming process

The different experiments point out that the dominant factor that governs the polymer foamability is the pressure drop in the die. Knowing the temperature dependent rheology of the different polymers, one can calculate the pressure drop in the die geometry (Figure 4). To obtain simple analytical formulations, we use a temperature dependent power law behavior which parameters are listed in Table 1. Referring to relation (4), the viscosity reduction due to gas content is considered by taking a shift factor $a_g(1.05) = 0.77$. The viscous dissipation may be neglected due to the limited pressure drop and each calculation is performed at the set melt cooler temperature. In the final capillary die the pressure drop writes:

$$\Delta P_{\text{cap}} = 2\,K \left(\frac{3m+1}{m}\frac{Q}{\pi}\right)^m \frac{L_{\text{cap}}}{{R_0}^{3\,m+1}} \qquad (10)$$

where Q is the flow rate, L_{cap} is the length of the capillary and R_0 its radius (see Table 3).

In the upstream convergent geometry, we use the lubrication approximations which provides a reasonable approximation of the pressure drop (Dealy and Wissbrun, 1990). It writes for a power law fluid:

$$\Delta P_{\text{conv}} = 2\,K \left(\frac{3m+1}{m}\frac{Q}{\pi}\right)^m \frac{L_{\text{conv}}}{3\,m\,(R_1-R_0)}\left[\frac{1}{{R_0}^{3m}} - \frac{1}{{R_1}^{3m}}\right] \qquad (11)$$

where L_{conv} is the length of the convergent and R_1 the inlet radius (see Table 3). These two contributions can be collected in a "global" pressure drop due to shear, labelled as $\Delta P_{\mathrm{shear}}$. In the sequel, we follow Cogswell approach (Cogswell (1972) which assumes that the flow motion is split in shear and extensional (or elongational) components. Therefore, the pressure drop can be decomposed in two different components labelled as shear pressure drop ($\Delta P_{\mathrm{shear}}$) and extensional pressure drop (ΔP_{ext}). The shear pressure drop is computed using the power law model which is well adapted to shear flow and therefore $\Delta P_{\mathrm{shear}} = \Delta P_{\mathrm{cap}} + \Delta P_{\mathrm{conv}}$. For the pressure drop due to extensional flow, a viscoelastic behavior has to be accounted for.

Following Cogswell approach (Cogswell (1972); Padmanabhan and Macosko (1997)) one may attribute the difference between the experimental pressure drop and the shear pressure drop to the extensional flow, $\Delta P_{\mathrm{ext}} = \Delta P_8 - \Delta P_{\mathrm{shear}}$. Figure 9 shows that the pressure $\Delta P_{\mathrm{shear}}$ calculated at the die inlet is lower than the measured one. The difference is especially important for branched polymers and at low foaming temperature. As Figure 2 shows that branched PPs have a more important elongational viscosity than linear ones, it is not surprising to obtain a more important ΔP_{ext} value for branched PPs than for linear ones.

Figure 9

The extensional pressure drop ΔP_{ext} is plotted as a function of temperature on Figure 10. It is interesting to note that the "extensional term" does follow an Arrhenius dependence (with the same activation energy as for the shear viscosity) at high temperature, but there is an important mismatch between ΔP_{ext} and the Arrhenius dependence as the foaming temperature is decreased. This effect is very important for the branched PP grades. For the linear PP grades, ΔP_{ext} follows the Arrhenius law, except for the minimal foaming temperature of the grade PPR-L.

At high temperature, we use Cogswell analysis (1972) revisited by Demay *et al.* (2018) to identify a mean elongational viscosity in the convergent. The mean elongation rate writes:

$$\dot{\varepsilon} = \frac{3\,Q}{\pi}\,\frac{\ln R_1/R_0}{R_1^3 - R_0^3}\,\frac{\sin^3\alpha}{1-\cos\alpha} \tag{12}$$

As the flow rate is constant for all experiments, the elongation rate is $\dot{\varepsilon} = 0.13\ s^{-1}$. The elongational viscosity is deduced from the excess pressure drop ΔP_{ext} by

$$\eta_e = \frac{\sigma_e}{\dot{\varepsilon}} = \frac{\pi\,\Delta P_{\text{ext}}}{Q}\,\frac{1-\cos\alpha}{\sin^3\alpha}\,\frac{R_0^2\ R_1^2}{(R_1 + R_0)\ln R_1/R_0} \tag{13}$$

At a temperature of $150\ °C$, it is assumed that there is no crystallization for the different PPs (160°C should be considered for PPR-B). The elongational viscosity calculated using Eq. 13 (considering the gas shift factor) ranges between 4.3 and $5\text{x}10^4$ Pa. s for both linear polymers. These values are in good agreement with the elongational viscosities deduced from figure 2 at an equivalent elongation rate and applying both temperature and gas shift factors. Experimental values for the branched polymers (implying the strain hardening) are larger than the estimated values (factor 5 to 7) but remain consistent.

Figure 10

Keeping in mind that the branched PP grades crystallize at a higher temperature than the linear ones, a partial crystallization of the polymer in the die could explain this departure from the Arrhenius thermal dependence observed for the branched polymer. The contribution of a crystallized fraction to the viscous shear contribution of the pressure drop in the die can be easily integrated by considering an additional shift factor linked to the presence of a crystallized volume fraction ϕ_C. Following Tanner (2002), this shift factor writes:

$$a_C = \left[1 - \frac{\phi_C}{B}\right]^{-2} \tag{14}$$

where $B = 0.54$ for a spherulitic structure (Tanner, 2002).

This shift factor is introduced at each foaming temperature in Eqs. 10 and 11 to calculate the shear pressure drop value $\Delta P^*_{\text{shear}}$ accounting for crystallization. A new extensional pressure drop value accounting for crystallized volume fraction is obtained as:

$$\Delta P^*_{\text{ext}} = \Delta P_8 - \Delta P^*_{\text{shear}} \quad (15)$$

This can be rewritten as:

$$\Delta P_8 = \left[1 - \frac{\phi_C}{B}\right]^{-2} [\Delta P_{\text{ext}} + \Delta P_{shear}] \quad (16)$$

The value of ϕ_C is then deduced for the different PPs as a function of the foaming temperature (Figure 11).

Figure 11

It appears for branched polypropylenes below a critical temperature (145 °C for PPR-B and 160 °C for PPH-B). Crystallized volume fractions as high as 18% have been calculated. No crystallization has been identified for linear polypropylene PPH-L. For PPR-L, a slight crystallized volume fraction (8%) has been identified at the lowest foaming temperature.

This result should be considered with caution because the calculation assumes a constant averaged crystallized volume fraction in the die, whereas crystallization should develop progressively between die inlet and die exit, and perhaps at the end of the melt cooler.

The presence of dissolved CO_2 in PP was reported by Li *et al.* (2011) to decrease the crystallization temperature. It is interesting to note that the extensional flow, even in presence of 1.05 wt% CO_2 (dissolved gas), leads to a large increase of the crystallization temperature (from 103.9°C (DSC data in Table 2) to 145 °C in the die for PPR-B, and from 120.4°C (DSC data) to 160 °C for PPH-B). The crystallization can be induced by the orientation and extension of polymer chains in the converging part of the die, phenomenon which can be combined with an isothermal crystallization of the chains in the die. The isothermal crystallization at temperatures larger than the crystallization temperature in presence of gas leads to the formation of nanocrystals which act as crosslinks between the chains (Lee and Park, 2014; Romero-Diez *et al.*, 2021). The presence of a crystallized fraction before the foaming process seems to have two effects. The presence of small crystals can induce a larger nucleation of gas bubbles (Wong *et al*., 2013), resulting in a larger number of smaller bubbles in the foam. This is illustrated in Figure 7 which compares the foam morphology at foaming

temperatures of 144.1°C and 137.7°C. The crystallized fraction also reduces the gas diffusion in the polymer (due a larger viscosity, or to the reduced diffusion of gas in the crystalline phase) and thus limits the gas escape, enhancing the foaming process.

5. Conclusions

The extrusion foaming behavior of linear and branched polypropylenes, using CO_2 as a blowing agent, has been investigated. As shown previously by several authors, branched PPs realize low density foams contrarily to linear ones. A thermomechanical model of the polymer flow in the die allows proposing a realistic scenario of PP foamability. In order to obtain a low-density foamed extrudate at die exit it is necessary to impose a high pressure drop in the die and, simultaneously, to insure a high viscosity at die exit to prevent gas to escape from the extrudate. This can be achieved by three physical phenomena, as proposed by Di Maio at the international conference PPS 37 (Iannielo et al. (2022)): (1) a sharp viscosity increase by temperature reduction, (2) strain hardening, (3) flow-induced crystallization. Di Maio referred to these phenomena for the late stages of the foaming process (bubble impingement and foam setting) to withstand the wall cell extension between bubbles and prevent the wall cell rupture to avoid cell coalescence. In the present case, the same physical phenomena are considered during the elongational flow in the die. They result in a sharp viscosity increase, and thus pressure drop increase when decreasing the foaming temperature in the extruder, prior to the foaming process. This should affect the pressure drop rate and thus the nucleation phase of the bubbles.

The two chosen branched PPs achieve a good compromise between these additional requirements. Their crystallization temperatures are higher than for their linear corresponding PPs. Their activation energy is higher which means that their viscosity will increase more when decreasing the temperature. At the same time, the elongational viscosity measurements show a marked strain hardening for branched PPs which is attested by an increased pressure drop in the convergent region

of the die. The corresponding linear PPs do not fulfill these requirements: A lower crystallization temperature, a lower activation energy for the viscosity, a lower Newtonian plateau and no strain hardening. However, as pointed out by Xu *et al.* (2007) it would be dangerous to conclude that linear PP are not suitable for foaming.

The proposed thermomechanical model brings new light to the foamability of polypropylenes with different architectures using online pressure and temperature measurements. A computed pressure drop is deduced from shear viscosity data. The difference between the die inlet measured pressure and the computed one defines an excess pressure drop, assigned to the elongational flow in the converging part of the die, at the different foaming temperatures. The physical origin of this "excess pressure drop" is threefold: Arrhenius viscosity dependance, strain hardening and crystallization. The two last contributions may be discriminated by introducing temperature and crystallinity shift factors. The thermomechanical model may be improved by introducing a more realistic rheological behavior adjusted on the shear and elongational viscosity measurements and accounting for an incremental crystallinity development in the die.

Annex

Differential scanning calorimetry crystallization curves for the different polypropylene grades are depicted in Figure A.

Figure A

References

Carreau, P. J., "Rheological equations from molecular network theories", Trans Soc Rheo, 16, 99-127 (1972)

Cogswell, F. N., "Converging flow of polymer melts in extrusion dies", Polym. Eng. Sci., 12, 64-73 (1972)

Cogswell, F. N., “Measuring the Extensional Rheology of Polymer Melts”, Trans Soc Rheo, 16(3), 383-403 (1972) doi:10.1122/1.549257

Cox, W.P. and Merz, E.H., “Correlation of dynamic and steady flow viscosities”, J. Polym. Sci., 28, 619–622 (1958)

Dealy, J. M. and Wissbrun, K. F., “Melt Rheology and Its Role in Plastics Processing - Theory and Applications”. Van Nostrand Reinhold, New York (1990)

Demay, Y., Abdesselam, Y., Castellani R. and Agassant, J. F., “Abnormal Behaviors in the Capillary Rheometry of Plastisol Formulations”, Intern. Polym. Proc., 33, 363-370 (2018)

Guo, Q.-P., Wang, J., Park, C. B. and Ohshima, M., “A microcellular foaming simulation system with a high pressure drop rate”, Ind. Eng. Chem. Res., 45, 6153-6161 (2006)

Guo, Q.-P., Wang, J. and Park, C. B., “A Comparison of CO_2 and N_2 Foaming behaviors of PP in a Visualization System”, Int. Polym. Proc., 35, 503-516 (2020)

Ianniello, V., Costango, S., Pasquino, R., Di Maio. E., “A heuristic approach to foamability”, Polymer Processing Society International Conference PPS37, Fukuoka, Japan (2022)

Lee, S.T., Park, C.B., editors of Foam Extrusion: Principles and Practice, Second Edition, CRC Press (2014)

Lee, P.C., Park, C.B., “Extrusion of high-density and low-density microcellular plastics” in: Foam Extrusion: Principles and Practice, Second Edition, Lee, S.T., Park, C.B. (Ed.), CRC Press. 435-488 (2014)

Li D.C., Liu T., Zhao L., Yuan W. K., “Foaming of isotactic Polypropylene based on its non-isothermal crystallization behaviours under compressed CO_2”, J. of Supercritical fluids, 60, 89-97 (2011) doi: 10.1016/j.supflu.2011.07.015

Mohebbi, A., Mighri, F., Ajji, A. and Rodrigue, D., “Current Issues and Challenges in Polypropylene Foaming: A Review”, Cellular Polymers, 34, 299-337 (2015)

Münstedt, H., Starý, Z., “Steady states in extensional flow of strain hardening polymer melts and the uncertainties of their determination”, J. Rheol. 57, 1065-1077 (2013) doi: 10.1122/1.4803932

Naguib, H. E., Park, C. B., Panzer U. and Reichelt N, “Strategies for achieving ultra-low-density Polypropylene foams”, Polym. Eng. Sci. 42, 1481-1492 (2002)

Naguib, H. E., Park, C. B. and Reichelt, N. “Fundamental foaming mechanisms governing the volume expansion of extruded polypropylene foams”, J. Appl. Polym. Sci. 91, 2661-2668 (2004)

Padmanabhan, M. and Macosko C.W., “Extensional viscosity from entrance pressure drop measurements”, Rheol. Acta 36(2), 144-151 (1997) doi: 10.1007/BF00366820

Park, C. B., Baldwin, D. F. and Suh, N. P., “Effect of the pressure drop rate on cell nucleation in continuous processing of microcellular polymers”, Polym. Eng. Sci., 35, 432-440 (1995)

Spitael, P. and Macosko, C., “Stain hardening in Polypropylene and its role in extrusion foaming”, Polym. Eng. Sci. **44**, 2090-2100 (2004)

Rainglet, B., Chalamet, Y., Bounor-Legaré, V., Delage, K., Forest, C. and Cassagnau, P., “Polypropylene foams under CO2 batch conditions: From formulation and rheological modeling to cell-growth simulation”, Polymer 218, 1-9 (2021)

Ramesh, N. S., “Foam growth in polymers” in: Foam Extrusion: Principles and Practice, Second Edition, Lee, S.T., Park, C.B. (Ed.), CRC Press. 213-238 (2014)

Raps, D., Köppl, T., de Anda, A. R., Altstädt, V.,”Rheological and crystallisation behaviour of high melt strength polypropylene under gas-loading”, Polymer, 55, 1537-1545 (2014) doi: 10.1016/j.polymer.2014.01.036

Raps, D., Köppl, T., Heymann, L. and Altstädt, V., “Rheological behaviour of a high-melt-strength polypropylene at elevated pressure and gas loading for foaming purposes”, Rheol Acta, 56, 95-111 (2017) doi: 10.1007/s00397-016-0988-6

Romero-Diez, S., Sung Kweon, M., Kim, E.S., Gupta, A., Yan, X., Pehlert, G., Park, C.B., Lee, P.C., “In situ visualization of crystal nucleation and growth behaviors of linear and long chain branched

polypropylene under shear and CO2 pressure", Polymer 213, 123215 (2021) doi: 10.1016/j.polymer.2020.123215

Salmang, R. and Pinsolle, F., "Polymères allégés en extrusion", Techniques de l'Ingénieur, AM3343 (2014)

Tanner, R.I., "A suspension model for low shear rate polymer solidification", J. Non-Newt. Fluid Mech., 102, 397-408 (2002)

Vega, J.F., Hristova D.G. and Peters, G. W. M., "Flow-induced crystallization regimes and rheology of isotactic polypropylene", J. Therm. Anal Calorim. 98, 655-666 (2009) doi: 10.1007/s10973-009-0516-3

Xu, Z., Xue, P., Zhu, F. and He, J., "Effects of formulations and processing parameters on foam morphologies in the direct extrusion foaming of Polypropylene using Single Screw Extruder", J. Cellular Plastics 41, 169-185 (2005)

Xu, Z. M., Jiang, X. L., Liu, T., Hu, G. H., Zhao, L., Zhua, Z. N. and Yuan, W. K., "Foaming of polypropylene with supercritical carbon dioxide", J. Supercritical Fluids 41, 299-310 (2007)

Yasuda, K. Y., Amstrong, R. C., Cohen, R. E., "Shear flow properties of concentrated solutions of linear and star branched polystyrenes", Rheol Acta, 20: 163-178 (1981)

Welle, A., Carpentier, J.F., Kirillov, E., Piola L. and Santoro, O., Patent WO 2022/029212 A1, TOTAL Research & Technology Feluy and Centre National de Recherche Scientifique (2022)

Zhang, H., Fang, Z., Liu, T., Li, B., Li, H., Cao, Z., Jin, G., Zhao, L. and Xin, Z., "Dimensional Stability of LDPE Foams with CO2 + i-C4H10 Mixtures as Blowing Agent: Experimental and Numerical Simulation", Ind. Eng. Chem. Res. 58, 13154-13162 (2019)

Table captions:

Table 1: Rheological parameters of the different linear and branched PP grades at reference temperature T_{ref} =170°C

Table 2: Crystallization temperatures and enthalpy, measurements performed at $10°C/mn$

Table 3: Die dimensions in mm.

Table 4: Temperature set values along barrel and gear pump

Table 5: Parameters of Eqs. (8) and (9) evaluated from Areerat et al. (2004)

Figure captions:

Figure 1: Shear viscosity curves of the different PPs at T=170°C.

Figure 2: Elongational rheology versus strain ε for the different PP grades at 170°C and $\dot{\varepsilon} = 0.1\ s^{-1}$. Troutonian viscosities of the linear grades were indicated for sake of comparison with the steady state elongational viscosities.

Figure 3: Physical foaming extrusion disposal. The sensors for temperature and pressure measurements are indicated.

Figure 4: Schematic drawing of the extrusion die geometry.

Figure 5: Pressure profile as a function of the foaming temperature T_m (PPR-B).

Figure 6: Relationship between foam density and pressure drop in the die for the four linear and branched polypropylenes. Dashed lines correspond to the theoretical density (Eq. 9).

Figure 7: Foam structure of the foamed extrudates for PPR-B at different foaming temperatures.

Figure 8: Foam structure of the foamed extrudates for PPH-B (a) and PPH-L (b) grades.

Figure 9: Comparison between the measured pressure drop ΔP_s and the calculated pressure drop in the capillary ΔP_{cap} and in the convergent ΔP_{conv} for the four grades.

Figure 10: ΔP_{ext} as a function of temperature for branched (circular symbols) and linear (square symbols) PPR grades. Continuous lines represent the respective Arrhenius thermal dependence of ΔP_{ext} starting from the largest melting temperature in absence of crystallization using the activation energy determined under shear.

Figure 11: Calculated crystallized volume fraction as a function of foaming temperature for the different polypropylenes

Figure A: Crystallization curves for branched grades on the left, for linear grades on the right

Tables:

	PPH-B	PPR-B	PPH-L	PPR-L
E_a (kJ/mol)	45.6	47.9	40.2	41.6
Power law				
K (Pa.s^m)	8600	8400	17100	17700
m	0.45	0.44	0.40	0.38
Carreau Yasuda				
η_0 *(Pa.s)*	21000	18000	12000	10000
λ (s)	4.19	3.32	0.47	0.35
b	0.47	0.49	0.82	0.79
m	0.45	0.44	0.40	0.38

Table 1: Rheological parameters of the different linear and branched PP grades at reference temperature T_{ref} =170°C

Polymer	Onset of crystallization (°C)	Crystallization peak (°C)	Crystallization enthalpy (J/g)
PPH-L	112.5	110.4	87.1
PPH-B	123.1	120.4	91.4
PPR-L	99.7	96.6	66.7
PPR-B	106.7	103.9	64.8

Table 2: Crystallization temperatures and enthalpy, measurements performed at $10°C/mn$

Convergent inlet radius $\boldsymbol{R_1}$	Convergent length $\boldsymbol{L_{conv}}$	Capillary radius $\boldsymbol{R_0}$	Capillary length $\boldsymbol{L_{cap}}$
25	50	1.5	1

Table 3: Die dimensions in mm.

T_1 (°C)	T_2 (°C)	T_3 (°C)	T_4 (°C)	T_5 (°C)	T_6 (°C)	T_7 (°C)
215	200	200	190	180	180	175

Table 4: Temperature set values along barrel and gear pump

H_0 (wt%/MPa)	0.14
ΔH_{sol} (J/mole)	-6.23×10^3
ρ_{CO_2} (kg/m^3)	1253
M_{CO_2} (kg/mole)	44.01×10^{-3}
ρ_{PP} (kg/m^3)	881.7
P_{atm} (MPa)	0.101325

Table 5: Parameters of Eq. (8) and (9) evaluated from Areerat et al. (2004)

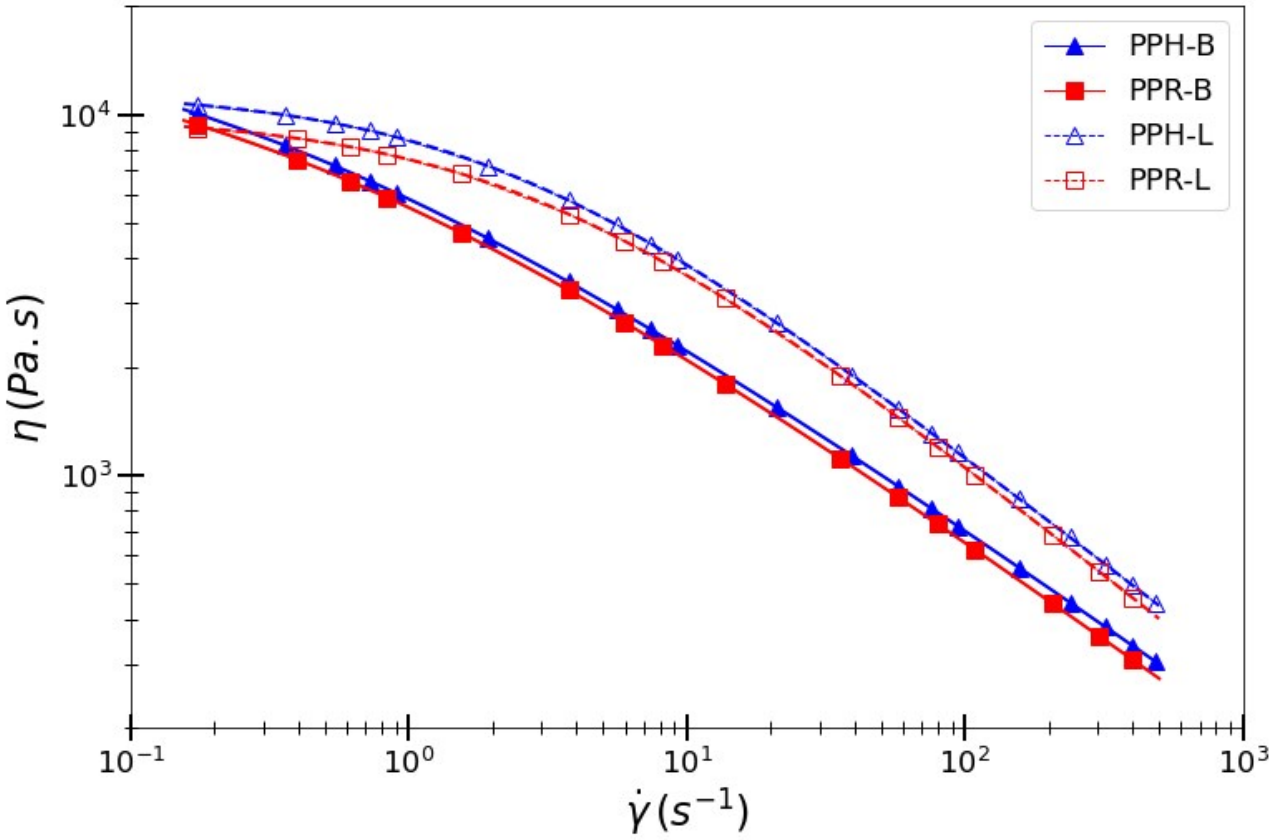

Figure 1: Shear viscosity curves of the different PPs at T=170°C.

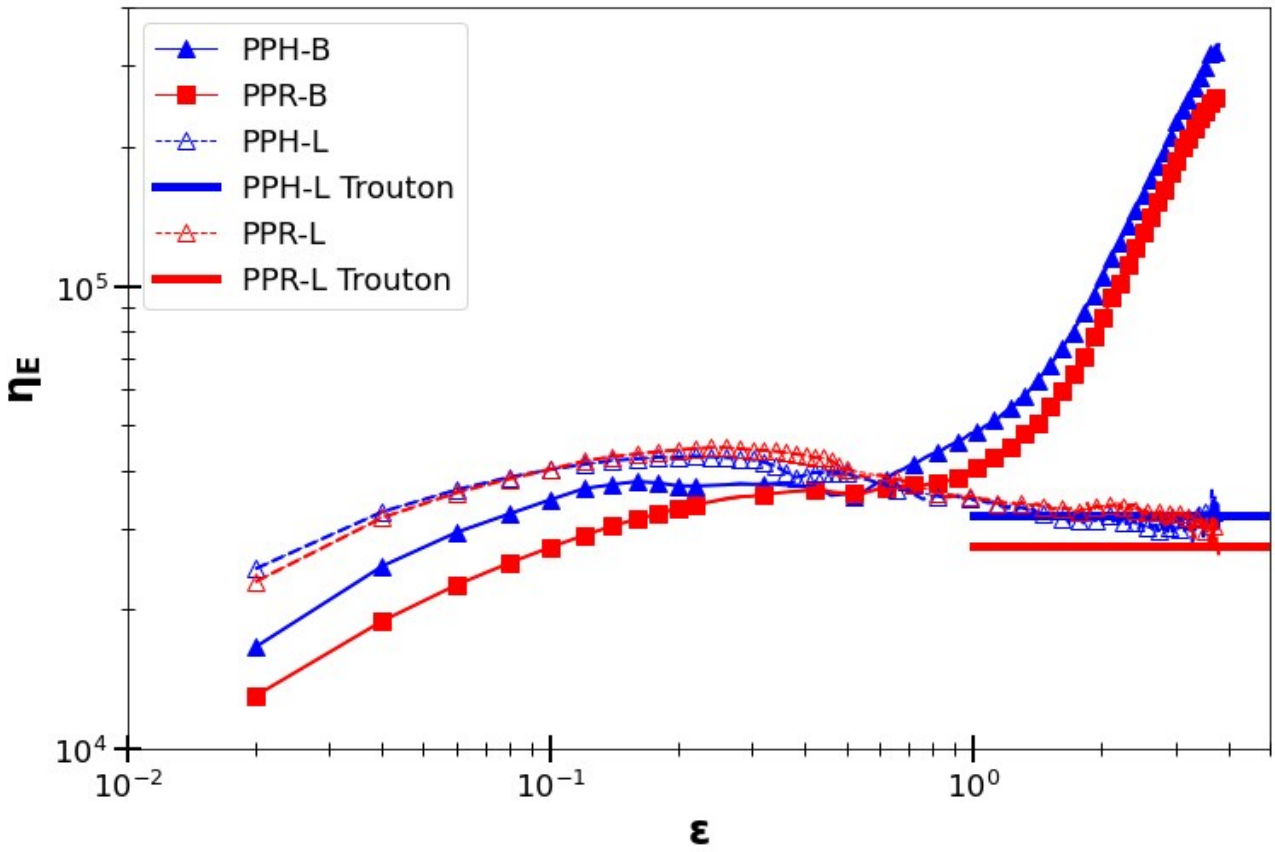

Figure 2: Elongational rheology versus strain ε for the different PP grades at $170°C$ *and* $\dot{\varepsilon} = 0.1\ s^{-1}$. *Troutonian viscosities (calculated from shear viscosities) of the linear grades were indicated for sake of comparison with the steady state elongational viscosities.*

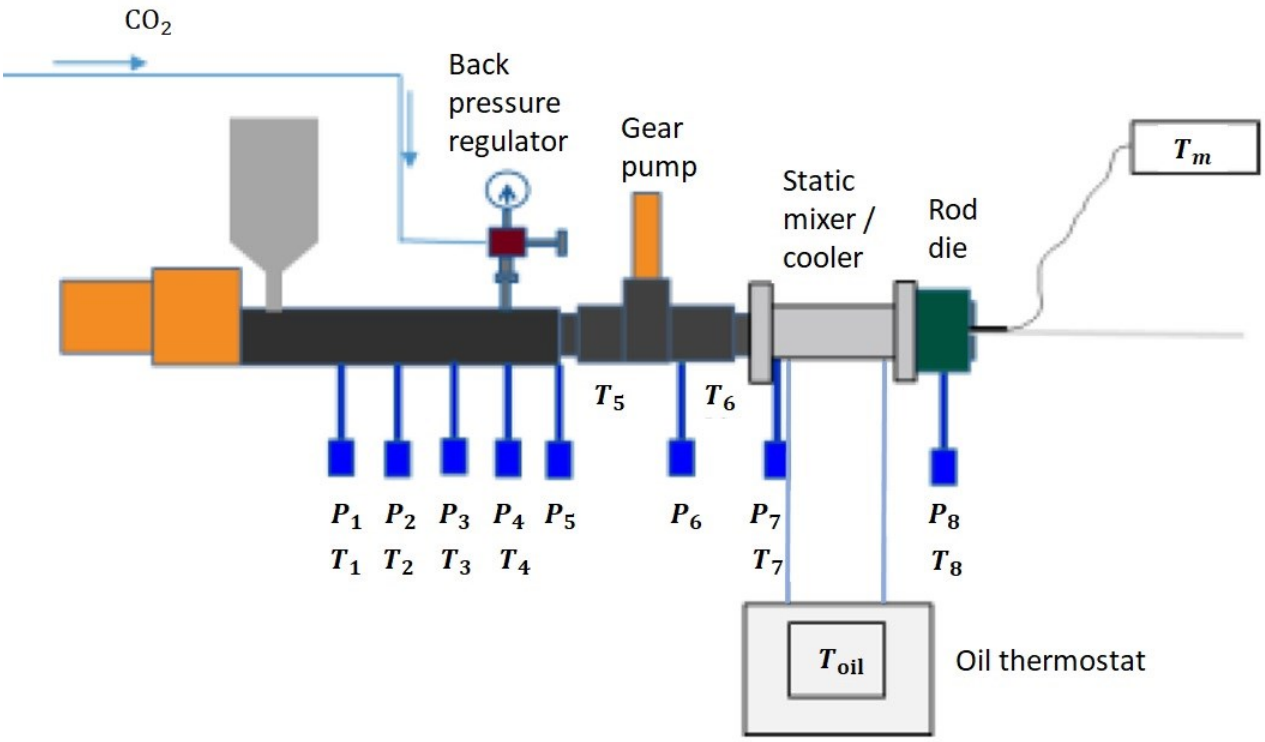

Figure 3: Physical foaming extrusion disposal. The sensors for temperature and pressure measurements are indicated.

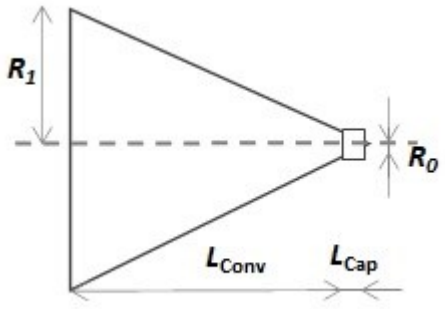

Figure 4: Schematic drawing of the extrusion die geometry.

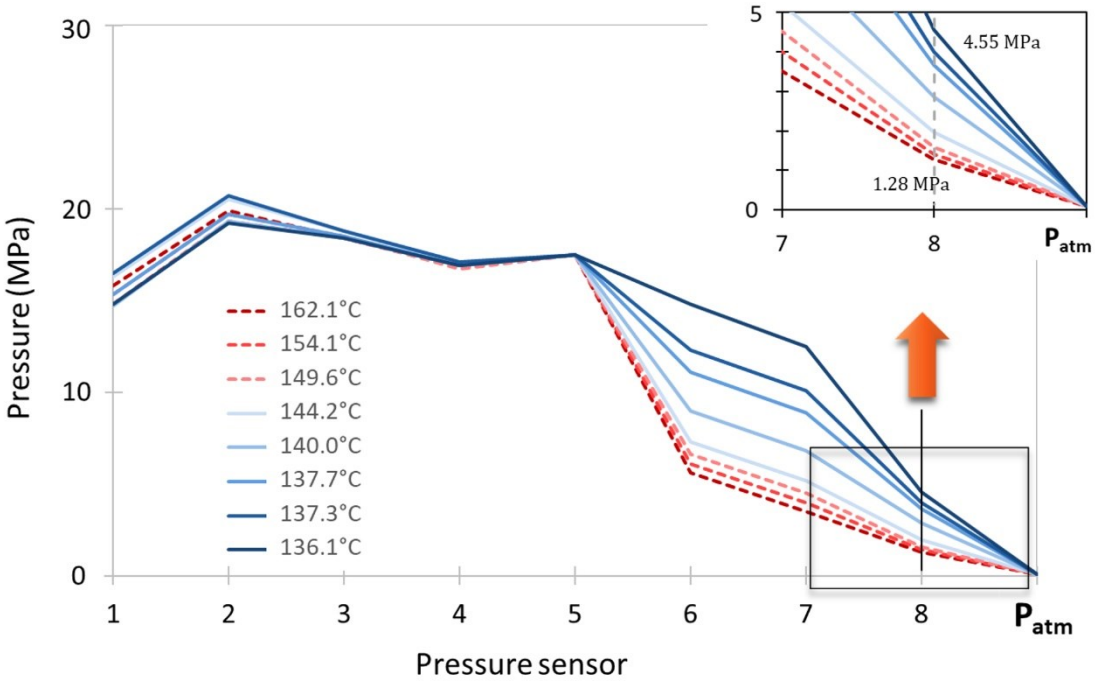

Figure 5: Pressure profile as a function of the foaming temperature T_m (PPR-B).

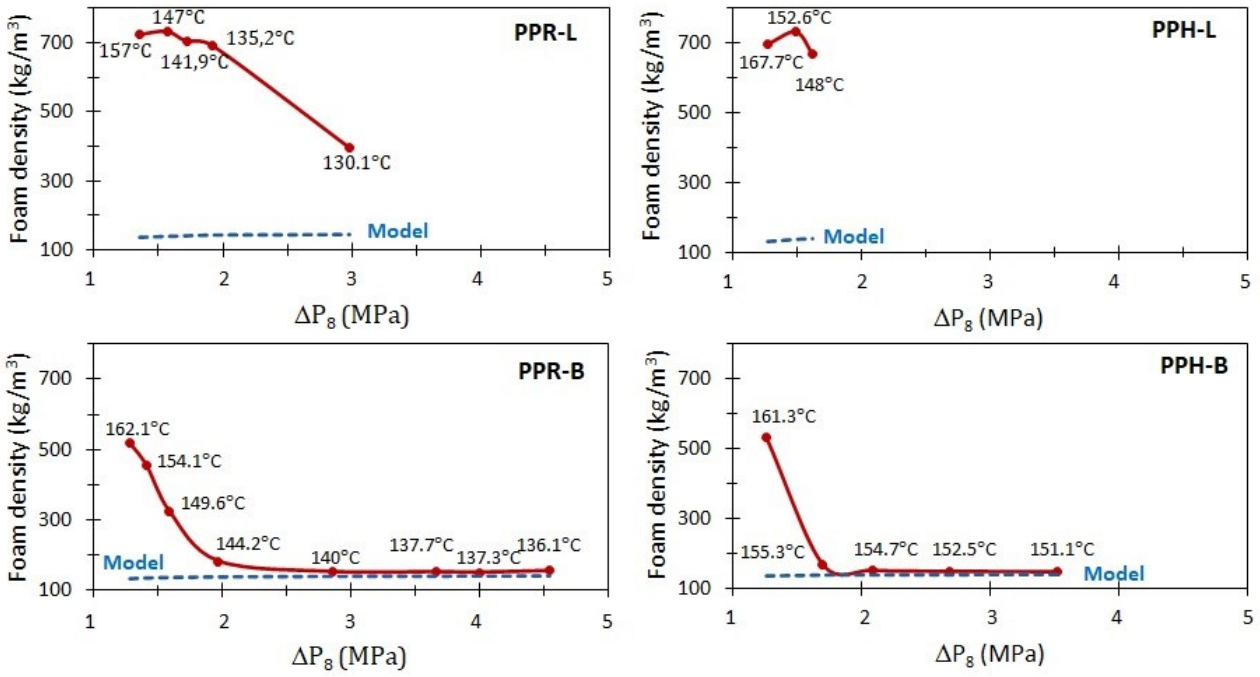

Figure 6: Relationship between foam density and pressure drop in the die for the four linear and branched polypropylenes. Dashed lines correspond to the theoretical density (Eq. 9).

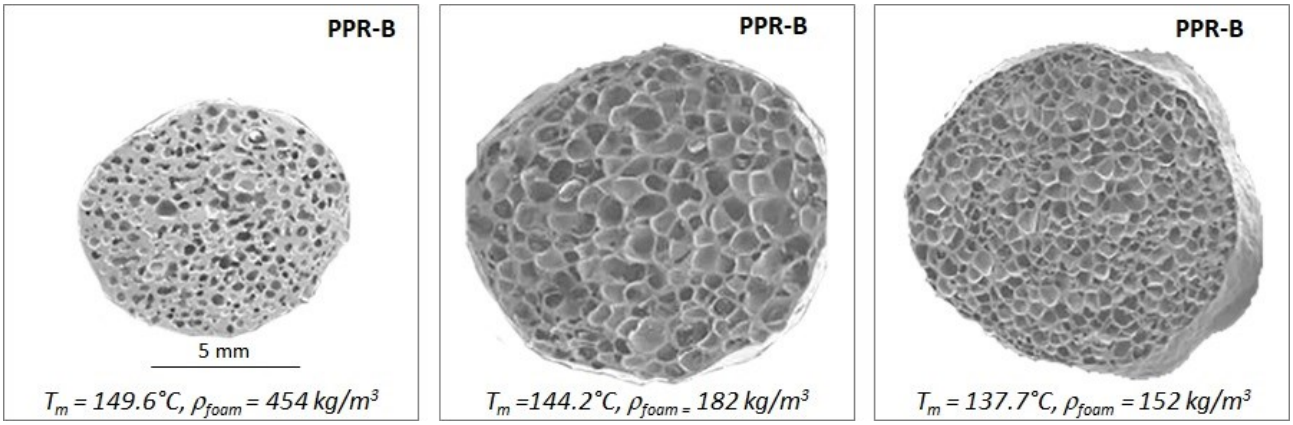

Figure 7: Foam structure of the foamed extrudates for PPR-B.

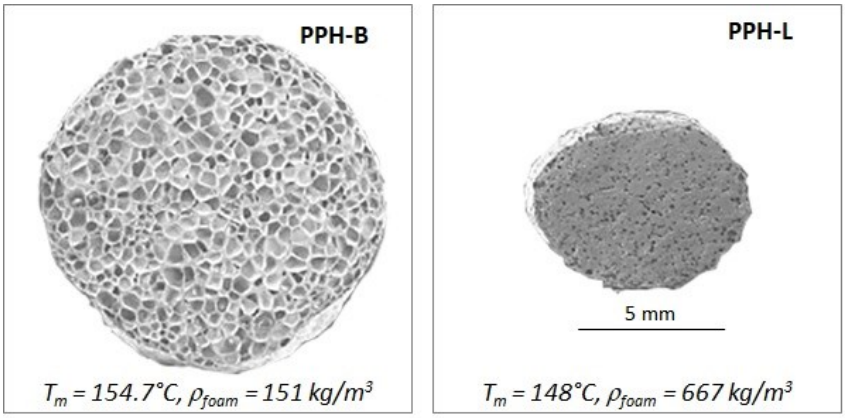

Figure 8: Foam structure of the foamed extrudates for PPH-B and PPH-L grades.

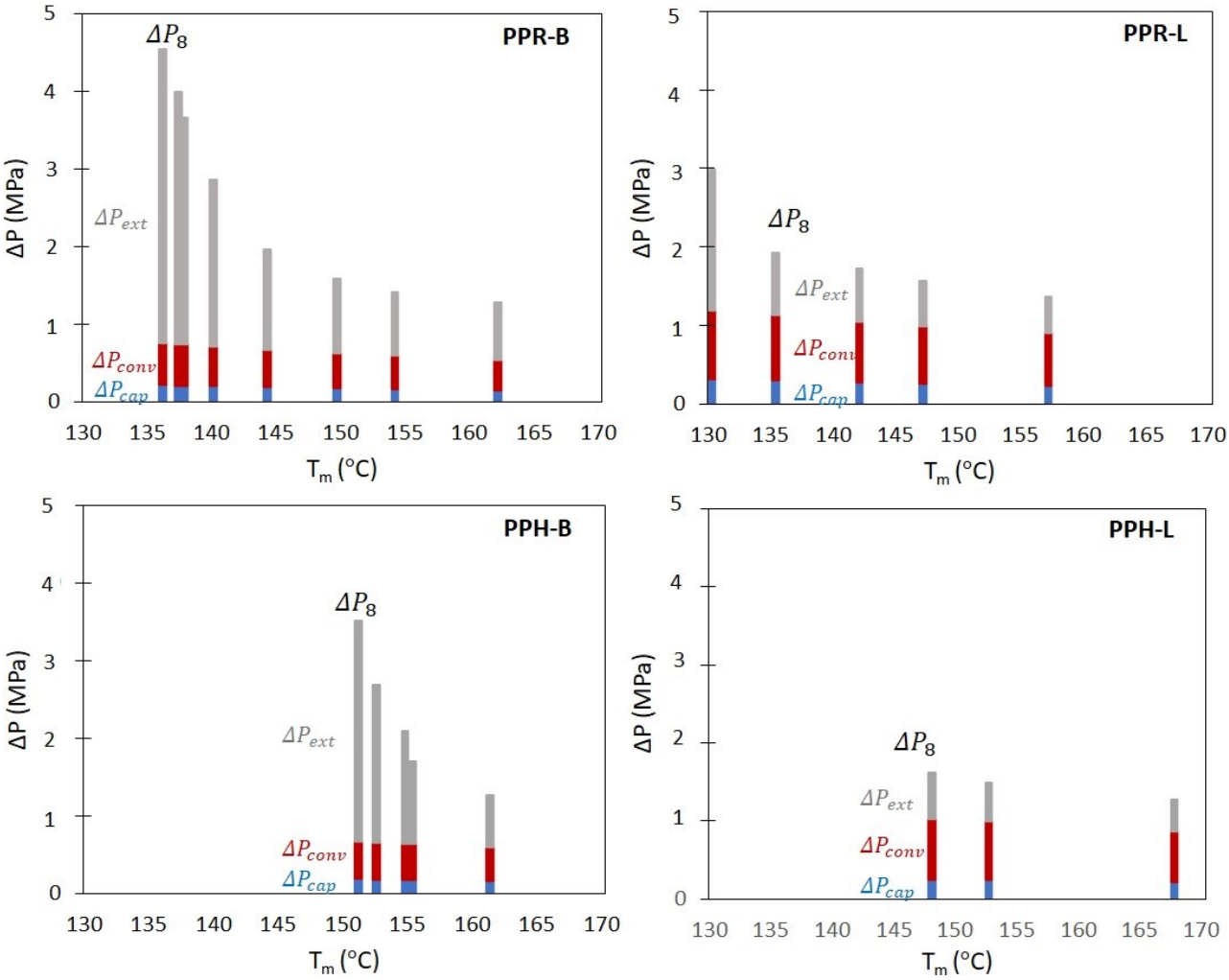

Figure 9: Comparison between the measured pressure drop ΔP_8 and the calculated pressure drop in the capillary ΔP_{cap} and in the convergent ΔP_{conv} for the four grades.

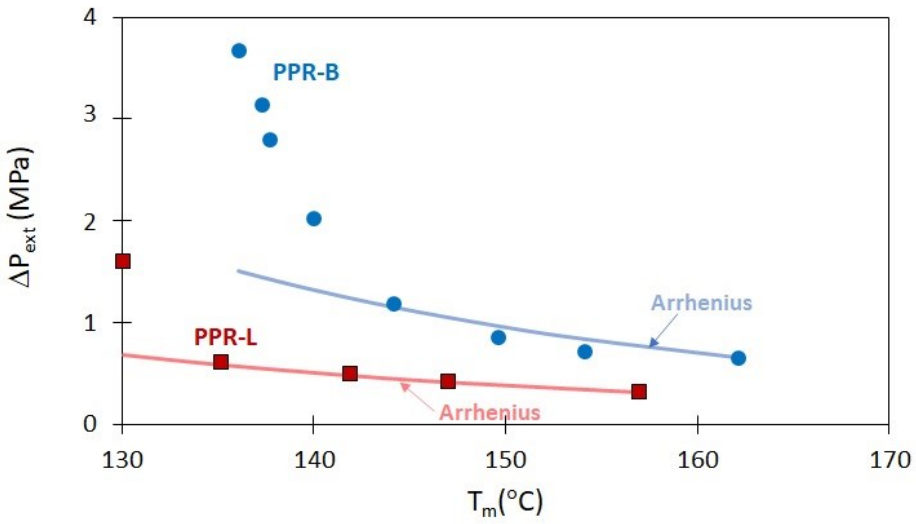

Figure 10: ΔP_{ext} as a function of temperature for branched (circular symbols) and linear (square symbols) PPR grades. Continuous lines represent the respective Arrhenius thermal dependence of ΔP_{ext} starting from the largest melting temperature in absence of crystallization using the activation energy determined under shear.

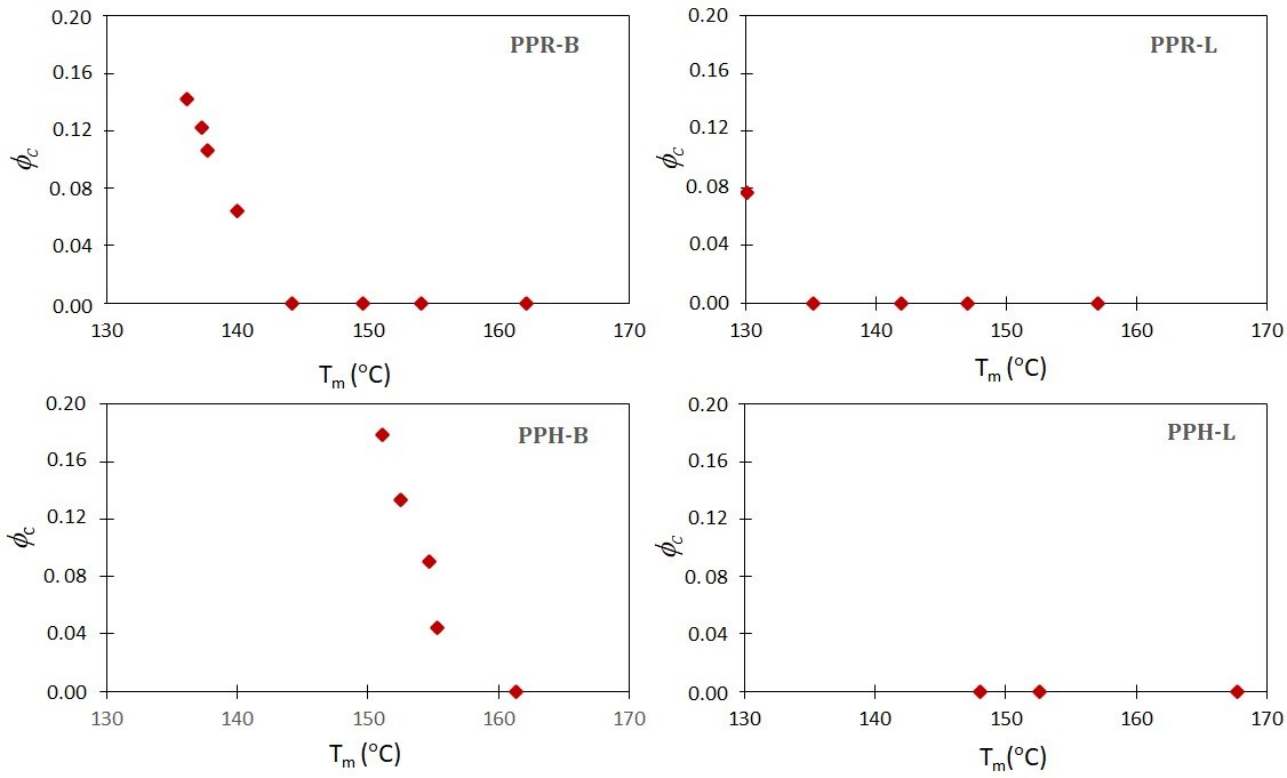

Figure 11: Calculated crystallized volume fraction as a function of foaming temperature for the different polypropylenes

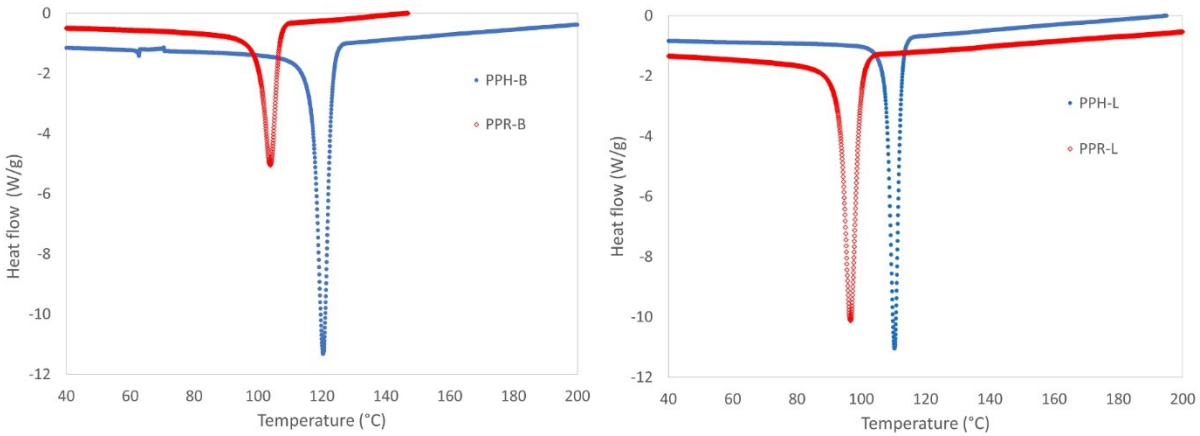

Figure A: Crystallization curves for branched grades on the left, for linear grades on the right.